YILDIRIM BEYAZIT UNIVERSITY

GRADUATE SCHOOL OF NATURAL AND APPLIED SCIENCES

Production of Doped/ Undoped ZnO Transparent Conductive Oxide Thin Film by Hydrothermal Method

M.Sc. Thesis by

Ahmet Yiğit Kurtuluş

Department of Metallurgical and Materials Engineering

July, 2021

ANKARA

Production of Doped/ Undoped ZnO Transparent Conductive Oxide Thin Film by Hydrothermal Method

A Thesis Submitted to

The Graduate School of Natural and Applied Sciences of Ankara Yıldırım Beyazıt University

In Partial Fulfillment of the Requirements for the Degree of Master of Science in Material Engineering, Department of Material Engineering

by

AHMET YİĞİT KURTULUŞ

July,2021

ANKARA

M.Sc. THESIS EXAMINATION RESULT FORM

We have read the thesis entitled "**Production of Doped/ Undoped ZnO Transparent Conductive Oxide Thin Film by Hydrothermal Method**" completed by **AHMET YİĞİT KURTULUŞ** under the supervisions of **Asst. Prof. Dr. MEHMET FATİH ÖKTEM** and **Prof.Dr.ABDULLAH YILDIZ**.We certify that in our opinion it is fully adequate, in scope and in quality, as a thesis for the degree of Master of Science.

Asst. Prof. Dr. Mehmet Fatih ÖKTEM
Supervisor

Prof. Dr. Abdullah YILDIZ
Supervisor

Assoc.Prof.Dr. Gülsüm TOPATEŞ
Jury Member

Prof.Dr. Sefer Bora LİŞESİVDİN
Jury Member

Asst.Prof.Dr. Yasemin ŞAFAK
Jury Member

Prof. Dr. Sadettin ORHAN
Director

Graduate School of Natural and Applied Sciences

ETHICAL DECLARATION

I hereby declare that, in this thesis which has been prepared in accordance with the Thesis Writing Manual of Graduate School of Natural and Applied Sciences

• Obtaining all data, information and documents within the framework of academic and ethical rules,

• All information, documents and evaluations are presented in accordance with scientific ethics and morality,

• All materials used are fully cited and referenced,

• No changes have been made on the materials used,

• All presented works are original,

and I agree to waive all my legal rights in any event contrary to the above statements.

Date: **Signature:**

Name & Surname: Ahmet Yiğit Kurtuluş

ACKNOWLEDGMENTS

I sincerely thank to my advisors Prof. Dr. Abdullah Yıldız and Assistant Prof. Dr. Mehmet Fatih Öktem for their great support and motivation during my study. Their vast knowledge and valuable suggestions are very important in the realization and success of this study. Thanks to the help they provided me, they helped me very much both during the research phase and while writing this thesis.

My thanks goes to Lect. Abdullah Atılgan for his help and support during the experiment phase.

I would like to express my deep respect and gratitude to my family, who always supported me and always motivated me throughout the study.

July, 2021 **Ahmet Yiğit Kurtuluş**

Production of Doped / Undoped ZnO Transparent Conductive Oxide Thin Film by Hydrothermal Method

ABSTRACT

In this study, undoped and W-doped ZnO nanostructures (NSs) are synthesized on glass substrates by hydrothermal method. The effects of the temperature (75-125^{o}C) employed during the synthesis and the W-doping on the structural, morphological, optical, and electrical properties of the NSs are examined. Raman spectra suggests that three clear phonon modes exist at around ~100, 330, and 435 cm^{-1} respectively and asymmetry ratio is sensitive to both the temperature and W-dopant. In the visible region, the NSs grown at 100^{o}C exhibit an average transmittance of 85.73%, which is relatively higher, among others. It is interesting to note that W-doping into ZnO results in a substantial decrease in sheet resistance. Combining a modest transmittance in the visible region, W-doped ZnO NSs can serve as a promising transparent conducting oxide (TCO) film and demonstrates a good balance of the tradeoff between transmittance and sheet resistance, which leads to a remarkable enhancement in the figure of merit (FOM).

Keywords: Zinc oxide, tungsten (W) dopant, nanostructures, hydrothermal method

Hidrotermal Metotla Katkılı / Katkısız ZnO Şeffaf İletken Oksit İnce Film Üretimi

ÖZET

Bu çalışmada, katkısız ve W katkılı ZnO nanoyapıları (NY'ler) hidrotermal yöntemle cam yüzeyler üzerinde sentezlenmiştir. Sentez ve W-katkısı sırasında kullanılan sıcaklığın (75-125^{o}C) NY'lerin yapısal, morfolojik, optik ve elektriksel özellikleri üzerindeki etkileri incelenmiştir. Raman spektrumları, sırasıyla ~100, 330 ve 435 cm^{-1} civarında üç net fonon modunun mevcut olduğunu ve asimetri oranının hem sıcaklığa hem de W-katkısına duyarlı olduğunu göstermektedir. Görünür bölgede, 100^{o}C'de büyütülen NY'ler, diğerleri arasında nispeten daha yüksek olan, %85.73'lük bir ortalama geçirgenlik sergiler. ZnO'ya W-katkısının tabaka direncinde önemli bir düşüşe yol açması ilginçtir. Görünür bölgede mütevazı bir geçirgenliği birleştiren W katkılı ZnO NY'ler, gelecek vaat eden şeffaf bir iletken oksit görevi görebilir ve geçirgenlik ile levha direnci arasında iyi bir denge göstermektedir.Bu da başarım ölçüsünde dikkate değer bir artışa yol açar.

Anahtar Kelimeler: Çinko oksit, tungsten (W) katkı maddesi, nanoyapılar, hidrotermal yöntem

CONTENTS

ETHICAL DECLARATION II

ACKNOWLEGMENTS III

ABSTRACT IV

ÖZET V

NOMENCLATURE VIII

LIST OF TABLES X

LIST OF FIGURES XI

CHAPTER 1 1

INTRODUCTION 1

1.1 Problem Statement 2

1.2 Aims of Research 3

1.3 Proposed Solutions of Thesis 3

1.4 Market Research 4

CHAPTER 2 6

LITERATURE REVIEW 6

2.1 Metal Oxides 6

2.2 Zinc Oxide (ZnO) 7

2.3 ZnO Doped 10

2.4 ZnO Doped With Tungsten 11

2.5 Manufacturing Method 12

2.5.1 Hydrothermal Method 12

CHAPTER 3 14

EXPERIMENTAL PROCEDURES 14

3.1 Sample Preparation 14

3.2 Characterizations 16

3.2.1 X-ray Diffraction (XRD) 16

3.2.2 Scanning Electron Microscope (SEM) 18

3.2.3 Atomic Force Microscope (AFM) 19
3.2.4 Raman Spectrometry 20
CHAPTER 4 22
RESULTS AND DISCUSSION 22
4.1 Sample Preparation 22
4.2 Characterization Results 23
4.2.1 X-ray Diffraction Results (XRD) 23
4.2.2 Atomic Force Microscopy (AFM) Results 24
4.2.3 Scanning Electron Microscopy (SEM) Results 26
4.2.4 Raman Spectroscopy Results 28
4.2.5 Ultraviolet-Visible Spectroscopy 30
4.2.5.1 Optical Characterization Results 30
4.2.5.2 Electrical Characterization Results 30
CHAPTER 5 33
CONCLUSION and RECOMMENDATIONS 33

NOMENCLATURE

Acronyms

AFM	Atomic Force Microscopy
SEM	Scanning Electron Microscopy
XRD	X-Ray Diffractometer
AR	Anti-Reflection
DI	De-Ionized
DP	Dopant Precursor
DR	Doping Ratio
FOM	Figure Of Merit
FWHM	Full Width at Half Maximum
PV	Photovoltaic
RMS	Root Mean Square
rpm	Revolution per minute
SEM	Scanning Electronic Microscope
SM	Solution Molarity
TCO	Transparent Conductive Oxide
ITO	Indium Thin Oxide Film
VIS	Optical Visible Range
TCF	Transparent Conductive Film
B	Boron
Ga	Gallium
Al	Alumium
LPCVD	Low Pressure Chemical Vapor Deposition
UV	Ultraviolet
ZnO	Zinc Oxide
AZO	Aluminum Zinc Oxide
GZO	Gallium Zinc Oxide
ZAD	Zinc Acetate Dihydrate
MEA	Monoethanolamine

HEX	Hexamethylenetetramine
ZNH	Zinc Nitrate Hexahydrate
T	Temperature
T	Optical Transmittance
TC	Texture Coefficient
Vmp	Voltage at Maximum Power Point
Voc	Open Circuit Voltage
R_{sh}	Sheet Resistance
D	Crystal Size
C	Crystal Constant
I_{max}	Peak Intensity
ω_0	Peak Position
E_g	Band Gap

Greek Letter Symbols

z	Absorption Coefficient
β	Full Width of Half Maximum (FWHM)
Φ	Work Function
η	Efficiency
λ	Wavelength
ε	Strain
μ_n	Electron Mobility
μ_p	Hole Mobility
σ	Electric Conductivity
Θ_B	Bragg Angle
ρ	Hole Mobility

LIST OF TABLES

Table 2.1 Mechanical, Electrical and Optical Properties of Zinc Oxide..... 9
Table 4.1 Parameters extracted from XRD and AFM measurements..... 23
Table 4.2 Peak parameters are estimated from the fitting Lorentzian function of E_2^{high} mode..... 29

LIST OF FIGURES

Figure 2.1 Connection of metal octahedra with corners, edges, and faces containing one, two and three oxygen ligands, respectively 7

Figure 2.2 The wurtzite crystal structure of ZnO with the lattice parameters a and c 8

Figure 3.1 Schematic diagram of the experimental process..... 15

Figure 3.2 Rigaku Miniflex 600 XRD measurement system..... 20

Figure 3.3 FEI QUANTA 400F brand SEM system..... 20

Figure 3.4 Q-Scope 250 brand AFM system..... 19

Figure 3.5 Horiba brand Raman Spectrometry 20

Figure 4.1 XRD pattern of ZnO NSs..... 28

Figure 4.2 7 a) Raman spectra of samples, b)Lorentzian fitted peaks of 435 cm-1.. 28

Figure 4.3 SEM image of the NSs (a) ZO75, (b) ZO100, (c) ZO125 and (d) WZO100. The size distribution histograms obtained from the SEM images for samples: (e) ZO75, (f)ZO100,(g)ZO125 and (h)WZO100…….28

Figure 4.4 7 a) Raman spectra of samples, b)Lorentzian fitted peaks of 435 cm^{-1}... 28

Figure 4.5 Optical transmittance of the NSs as a function of wavelength. The inset shows a Tauc plot of the optical transmittance spectra of the NSs……..28

CHAPTER 1

INTRODUCTION

Semiconductor materials are of great importance in the development and survival of technology. Semiconductors, which have a wide variety of working and usage areas, form the basis of many devices we use. The importance of semiconductors is increasing day by day due to the contribution of researches in the development of new technologies to human life. Semiconductor materials are considered to be superior to other materials due to their optical and electrical properties. The researches and impressive features of scientists to discover nanomaterials used in technological applications create great motivation. Due to their optical and electronic properties, fields such as microelectronics and optoelectronics are frequently preferred. Recently, technology and scientists have been studying the properties and applications of semiconductor transparent and conductive thin films [1].

Semiconductor transparent and conductive oxide thin films are in the form of composite structures containing at least one or two metallic elements. The reason why semiconductors are transparent and conductive oxide thin films are preferred, and the parameters considered in the characterization of both optical and electrical properties are the crystal structure, the atomic number and formation of the metal cations, the arrangement morphology of the atoms and the defects in the structure [2]. Semiconductor transparent and conductive oxide thin films use additives to achieve the desired properties. Especially in doping made with metallic elements, there is a decrease in electrical resistance as well as an effect in the direction of dulling in optical properties. Therefore, the element to be used in the additive and the amount of use are critical as a result of the production.

The forms of doped ZnO, In_2O_3 and CdO, which are generally preferred in semiconductor transparent and conductive oxide thin films, are more dominant. Apart from these forms, it is seen that they are preferred in ternary compound structures. Based on the studies conducted, the results of Sn-doped In_2O_3 (ITO) and F-doped SnO_2 transparent conductive oxide thin films make it more preferable than others. However, the high cost due to the lack of In causes new searches to find a new alternative. The

critical parameters for the search for a new alternative are that electrical resistance should be less than 10^{-4} Ωcm and the extinction coefficient k in the optical visible range (VIS) be less than 0.0001. In the last case of the studies for the alternatives and, in the light of the experimental results, semiconductor transparent and conductive oxide thin films formed in ZnO: Al and ZnO: Ga materials are more emphasized. Although the desired level results cannot be obtained in the studies, the aim is to reach the target with different production methods and additions. It is aimed to create a new option in alternative studies. Although the desired level results cannot be obtained in the studies, the aim is to reach the target with different production methods and additions. It is aimed to create a new option in alternative studies.

1.1 Problem Statement

Semiconductor transparent and conductive thin films are in the form of compound structures formed by combining one or two metallic elements using a suitable method. Semiconductor materials have a great importance in the development of technology and reaching today's technology level. Semiconductors, which have a wide variety of working and usage areas, form the basis of many devices we use. Semiconductors preserve their reality and place in human life due to the contributions of studies and researches to human life.

These materials are considered superior to other materials due to some optical and electrical properties. Scientists' research to discover nanomaterials used in technological applications and their impressive properties has created a great motivation. Due to their optical and electronic properties, nanomaterials find application in fields such as microelectronics and optoelectronics. Recently, one of the topics that technology and scientists have focused on is the properties and application areas of semiconductor transparent thin films.

Semiconductor and semi-transparent films are especially needed in the production of transparent electrodes found in optoelectronic devices. Due to the scarcity of indium and its high price, a new alternative was sought for these films. As a result of this search, transparent thin film production studies are carried out at least as much as ITO performance.

1.2 Aims of Research

The most distinguishing features of semiconductor transparent and conductive thin films are both their electrical and optical properties. These electrical and optical properties are directly affected by parameters such as crystal structure, quality of metal cations, atomic arrangement, morphology, and imperfections. Since the desired formation of both conductive and transparent structures does not occur naturally, it is aimed to provide these properties with doping. The use of Sn-doped In_2O_3 (ITO) and F-doped SnO_2 thin films are more preferred [2].

The most striking aspects of semiconductor transparent thin film coatings are their structure, surface properties, electrical resistance and optical properties. Because of their optical and electrical properties, these films are highly emphasized and studied.

The electrical resistances of the new semiconductor transparent and conductive thin films are intended to be less than 10^{-4} Ωcm and the extinction coefficient k in the optical visible range (VIS) to be less than 0.0001 due to the large optical band gap that can be greater than 3 eV. Currently, ZnO: Al and ZnO: Ga (AZO and GZO), semiconductor transparent and conductive thin films are good alternatives to ITO, but still the desired level of results has not been achieved [1].

The main purpose of this study is to produce an alternative semiconductor transparent and conductive thin layer by using dopant with tungsten metal, which is produced with the hydrothermal method, has just started to be studied amongst the conducted research.

1.3 Proposed Solutions of Thesis

There are studies to find a new alternative to IZO TCOs, which have been used dominantly in the last thirty to forty years, due to the lack of indium and high cost. Since the ideal level of transparency and conductivity has not been reached until this time, efforts to find a new alternative continue. The ZnO material, which is frequently preferred as an alternative to IZO TCOs, will deal with temperature, dopant ,pH parameters and TCO thin film production will be done with the hydrothermal method instead of the frequently preferred chemical spraying method. This study aims to provide an alternative to the existing solar cells by reaching the optimum level of

transparency and conductivity. ZnO semiconductor, which has a wide range of research and development of nanotechnological applications, is a candidate for materials that are widely studied. Due to its wide gap energy range, ZnO can be used in the construction of various devices. Since the crystal structure of ZnO is in hexagonal wurtzite structure, its electrical, morphological, optical properties can be changed by heat treatment or by making various additions. Because of these important properties, ZnO thin films are generally preferred recently. It has been observed that it is doped with many different types of elements as additive atoms [2].

In the present work, it is aimed to produce optimum transparent and conductive thin film by considering the dopant, temperature and pH parameters of ZnO thin films produced by the hydrothermal method, instead of the frequently used chemical spraying method. Using the ideal thin film parameters obtained, it is aimed to produce a new alternative to the existing literature by producing solar cells.

In addition, the thesis will be an interdisciplinary quality, as the master's thesis will work together in materials engineering and energy systems.

1.4 Market Research

The transparent conductive films market has grown significantly in recent years due to the increasing population of high-end displays, smartphones, tablets, smart watches and other smart electronic devices. TCOs find great application in these electronic devices and the increasing number of these devices for both personal and commercial use positively affects the market. In addition, the growing demand for touch-enabled panels in many industries is driving the transparent conductive films (TCFs) market. In recent years, the production technology for TCFs has greatly improved in terms of flexibility, strength, slenderness, reflection limit and increased power efficiency; this provides a traction to the general TCFs market.

TCFs have been used in electronic devices for over forty years and have seen many technological advances in terms of the materials used. Today, CNT and graphene materials are adopted by various transparent conductive film manufacturers due to the advantages they offer. In terms of application areas, the TCFs market is expected to be

significantly adopted in the production of smart glass or electro-chromic glass for solar panels and smart windows.

Geographically, the market is expected to witness consistency in North America due to the acceleration in demand for smartphones and the burgeoning consumer electronics industry. Asia Pacific is expected to witness high growth, mainly due to the intensification of electronic device manufacturing in China and Japan. Tech expert Canatu Oy recently announced that it has signed multiple contracts to supply automakers in the US with conductive transparent films, including applications on in-car touchpads for control panels and entertainment system functions on steering wheels or backrests.This has increased the demand for infotainment systems and human-machine interface products to replace buttons, switches and buttons with stylish integrated capacitive sensing into unique and stylish 3D on-vehicle surfaces. Major vendors in the transparent conductive film industry include 3M, Cambrios Technologies Corp., Canatu Oy, DONTECH Inc., DuPont, Eastman Kodak, Fujifilm, Nitto Denko Corporation, Pike & Company, Rolith Inc. and Toyobo.

The global transparent conductive films Market reached US $ 2.4 billion in 2019 and is expected to reach US $ 5.1 billion by 2027, at a compound growth rate of 9.88% over the forecast period [3].

TCF market is expected to grow to USD 5.86 billion by 2020, reaching a compounded annual growth rate of 17.2% in the 2014-2020 forecast period. The transparent conductive films market refers to the production and application of TCF panels on glass or film. The TCF market in this report includes both glass and film-based transparent conductors. This market is inherently highly fragmented and complex. There are many players that create a perfect competitive environment. The market is growing primarily due to the increasing demand for touch devices and the introduction of tablet and tablet PCs. OLED lighting, OPV, and DSSSC are also potential markets, but are expected to experience slower growth over the forecast period. The main reason for this slow growth may be the current competition and uncertainty in demand for it [4].

CHAPTER 2

LITERATURE REVIEW

2.1 Metal Oxides

The basic structural unit of Fe, Mn, Al, and Ti oxides are cationic metal centers bound to six oxygens. If one drastically reduces the size of the oxide minerals, hydroxides, oxyhydroxides are found in special forms in nature and are in the hydrated form of the elements Si, Fe, Mn, Al and Zn. Most oxides are found in soils except SiO_2 and TiO_2, which are mostly primary minerals. Fe^{+2}, Mn^{+2}, Ti^{+4}, Al^{+3} and Si^{+4} metal cations are formed from silicates by the effect of air. Of the cations with a valence of 2, Mn and Fe are oxidized and hydrolysed. While hydrolyzing, oxide minerals precipitate. Al^{+3} and Si^{+4} tend to form secondary aluminosilicate clay minerals. Special conditions are required for the formation of Al and Si oxides. All of the oxides have low pH values in the soil. Alkalis contains approximately 50% metal oxides in alkaline soils and highly weathered soils.

Fe, Mn, Al and Ti oxides have reactive and high surface areas that enable strong bonding with oxyanions and metal cations. Some Mn oxides have strong oxidizing power and degrade organic pesticides. Therefore, they can change the toxicity of heavy metals and ensure the formation of organic substances in the soil. Unlike the Mn element, Si oxide is chemically inert towards crystals with sand size.

The basic structural properties of Fe, Mn, Al, and Ti oxides have six oxygene-bound cationic structures. The size of the cationic oxygen atoms can change geometrically. Octahedron geometric structure is seen if the size of the oxygen is reduced to cations (Figure 2.1). Octahedra can be connected to each other in three ways that share oxygen corners (1O), shared edges (2O) or faces (3O). While many oxide minerals such as goethite contain only the first two types of linkage, Fe oxide contains all three of the hematite. By bonding with four oxygens, silicon can form tetrahedron geometric shapes. While the tetrahedron forms a structure, atoms can only bond at the corners.

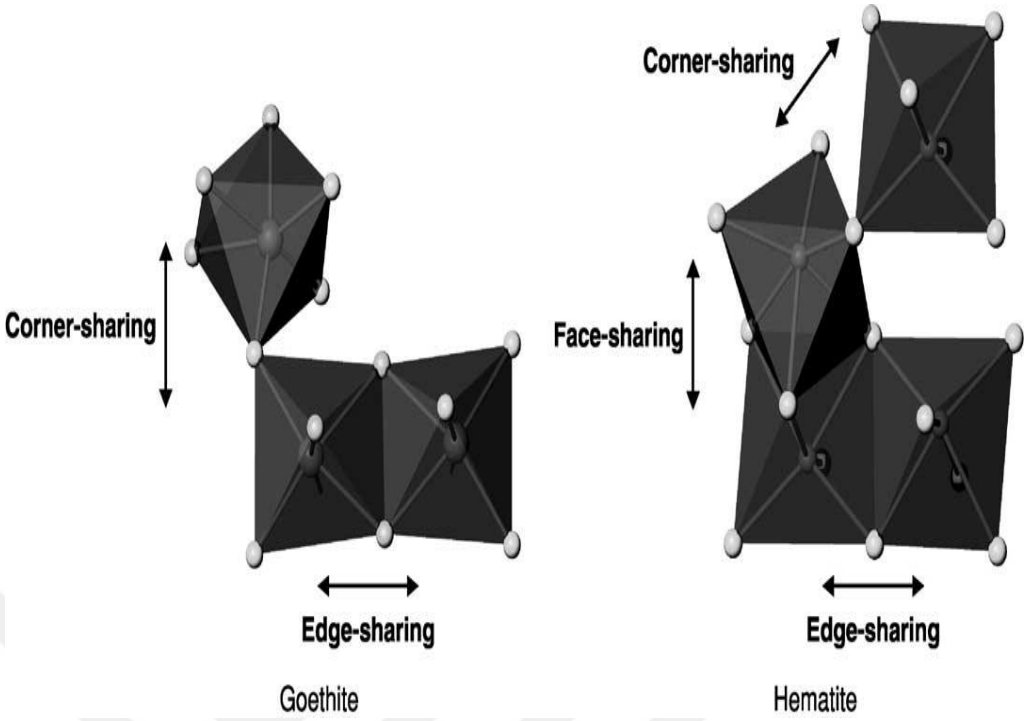


Figure 2.1 Connection of metal octahedra with corners, edges, and faces containing one, two and three oxygen ligands, respectively [5]

2.2 Zinc Oxide (ZnO)

ZnO is a direct broadband-spaced semiconductor material typically 3.37 eV [6] at room temperature that crystallizes in a wurtzite structure (Figure 2.2). It can be grown as single crystal or polycrystalline material in cast or thin film form. ZnO is characterized by high transparency for visible light, high electron mobility, high thermal conductivity, large free exciton binding energy, large piezoelectric constants, highly sensitive surface conductivity to the presence of adsorbed species, and many others. Additionally, the band gap of ZnO can be designed by adding Mg or Cd. An increase and a decrease in band gap can be obtained by adding Mg to ZnO and Cd to ZnO, respectively. Medium density MgZnO and CdZnO alloys assume the wurtzite structure of ZnO with band gaps in the range of 2.3 to 4.0 eV [7,8].

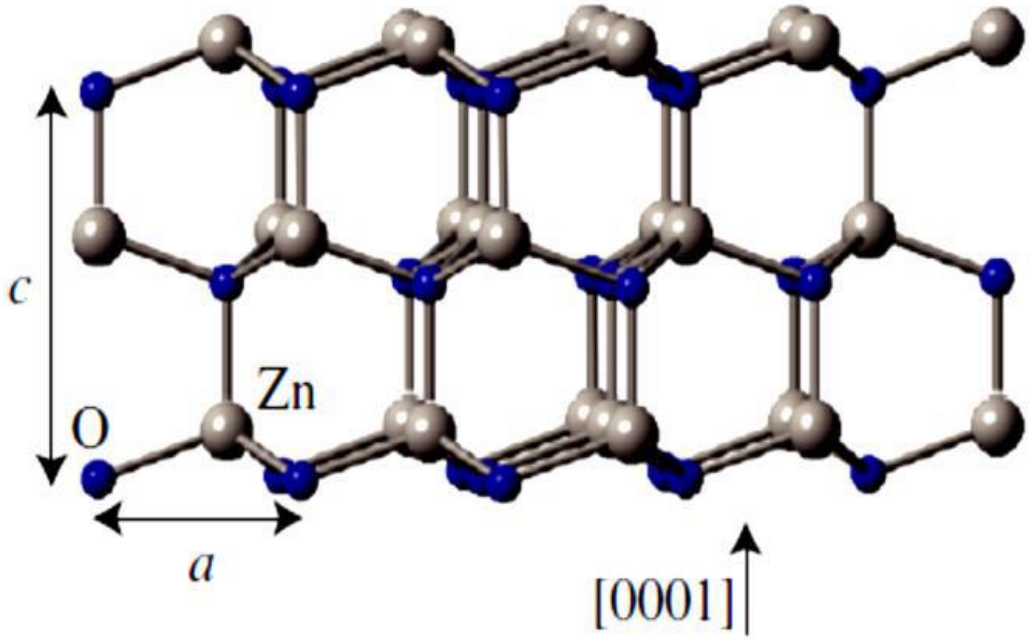


Figure 2.2 The wurtzite crystal structure of ZnO with the lattice parameters a and c [11]

N-type conductivity occurs due to the imperfections of undoped ZnO. These imperfections of chain oxide are due to the lattice structure. The cage structure contains cavities, spacers and antisides. Natural imperfections of ZnO directly affect their electrical and optical properties, and these imperfections also affect doping efficiency, minority carrier life and luminescence properties. Doping can be made with elements of Boron (B), Aluminum (Al), Gallium (Ga) and Indium (In) to create n-type conductivity in ZnO. Thanks to these elements, zinc oxides can act as shallow rotors, increasing the n-type conductivity. In experimental studies, carrier concentrations up to $8x10^{20}$ and $3.7x10^{20}$ cm^{-3} were observed for Al and Ga doped ZnO [9,10]. It has been observed in studies that it is very difficult to create p-type conductivity by doping of ZnO. Stable and reproducible p-type zinc oxide production has not been made yet, and the roadmap for the solution of the problem has not been revealed [12]. Significant changes occur not only in the electrical properties but also in the optical properties by adding zinc oxides. The transparency is directly affected by doping.

ZnO material has many distinctive features and a wide range of uses. Theoretically, ZnO are preferred for optoelectronic applications due to their wide band gaps and UV properties. With its other features, it is also frequently preferred in thin film transistors, photodiodes, thin film solar cells and gas sensors. ZnO can be used for different

purposes in the areas where they are used. For example, it can act as an active n-type conductive layer and a transparent window in transparent and conductive oxide films.

ZnO in single crystal structure with high purity are especially required in advanced applications and technologies. ZnO are generally used in polycrystalline films with lower crystal quality or purity. In the production of chain oxide polycrystalline films, they can be produced by spraying method, low pressure chemical vapor deposition (LPCVD), atomic layer deposition (ALD), chemical spray pyrolysis, electrochemical deposition and sol-gel synthesis.Among these methods, the sol-gel method is preferred more because it can be controlled more easily and can be produced at lower temperatures. At the same time, the sol-gel production method makes it possible to produce better coating in large area samples, homogeneous and purity production. Having a more affordable cost of production with the sol-gel method provides an extra advantage.

Table 2.1 Mechanical, Electrical and Optical Properties of Zinc Oxide [13]

ZINC OXIDE MECHANICAL PROPERTIES		**ZINC OXIDE ELECTRICAL& OPTICAL PROPERTIES**	
pH	6.95	Dielectric Constant	8.5
Density (g/cm^3)	5.6	Band Gap (eV)	3.4
Melting Temperature (C^o)	1974	Intrinsic Carrier Concentration (cm^3)	<106
Young Modulus (GPa)	122	Electron Mobility (cm^2/Vs)	200
Bulk Moduli (GPa)	143	Hole Mobility (cm^2/Vs)	180
Shear Modulus (GPa)	45	Refractive Index	2.013
Poisson Ratio	0.358		
Mohs Hardness	4		

2.3 ZnO Doped

Thin film studies produced with doping of ZnO are mostly preferred by researchers working in this field. ZnO have a wide morphological structure, high electron mobility and n-carrier properties. Thanks to these features, it is frequently preferred in applications such as memory devices, spintronics, optoelectronic devices, solar cells, and sensors. Apart from the existing studies, it is thought that it may be beneficial to try it on different multi-functional platforms thanks to its features.

It is often a preferred method to improve the electrical and optical properties by doping ZnO. It is formed by ion transfer from the element contributed to the cage structure in the doping made to ZnO. It has been determined that it is beneficial to modulate energy band gaps due to the photocatalytic properties of zinc oxides. The ions of the doped element by ZnO doping may cause conditions such as weakening of ferromagnetic behavior and degradation in aqueous environments. In addition, it has been observed in the studies that the electromechanical reaction may cause modulation in the structure of ZnO.

The physical and chemical properties of ZnO change by doping. These varies according to the properties of the added element. Electronegativity of zinc oxide, size and coordination of ions can be changed with doping. With the doping, a new functionality occurs in the structure of the zinc oxide.

When the ZnO is doped with rare earth or lanthanide elements, these elements are often preferred because the electronic band structure changes. Cerrato et al. [14] made such a doping and by studying the UV radiation of ZnO, they concluded that photogenerated charge carriers were recombined very quickly. When the element used in this study is utilized as a photocatalyst, a low quatum efficiency has been obtained. The use of lanthanide in the 4f configuration has been found to increase the recombination time in electron spaces [15]. Increasing the recombination time provides the development of photocatalic properties in antimicrobial activities as well. As an example, it has been concluded that zinc oxide nanorodes directly improve their photocatalytic properties in doping with cerium and are more efficient than titanium dioxide (TiO_2) used as comparative sample [16]. In the light of this information, the

use of rare earth elements is more preferred to improve the photocatalytic and optical properties of ZnO materials.

They are also frequently preferred transition elements in the doping of zinc oxides. Elements such as cobalt, chromium, Iron, manganese and copper are often known as preferred transition elements. It is known that very interesting results occur when zinc oxide is doped with transition elements. Research on transition element doped ZnO is of great interest as this material can function as a diluted magnetic semiconductor. As with rare earth elements, transition elements have no effect on zinc oxide in their ferromagnetic behavior, but changes in both electrical and optical properties are observed. They also affect properties such as oxidation state, ionic diameter, and electronegativity [17].

2.4 ZnO Doped With Tungsten

ZnO have a wide morphological structure, high electron mobility and doping method to make them more advantageous. Many studies are carried out with ZnO and doping is made with many different elements. It is aimed to achieve optimum production by making changes in electrical, photocatatic properties, grain sizes and morphological structures by introducing ion into the lattice structure of ZnO by doping.

There are some critical parameters for the combination of electrical conductivity and optical transparency expected in semiconductor transparent and conductive thin films. The crystal structure, quality of metal cations, atomic arrangement and settlement parameters are of great importance. ITO thin films have reached the most desired values in terms of electrical and optical performance in the studies, but ZnO is seen as the most important alternative because of indium scarcity and its cost. Therefore, it is aimed to reach the desired level by choosing new elements for new production methods and doping.

In our study, semiconductor transparent and conductive thin film was produced by making tungsten element as doping. A decrease in the tungsten doping band gap value, recrystallization formation in the crystal structure occurs. The rate of doping changes some values of tungsten doped on ZnO. As the doping rate increases, grain size and grain morphology change. After the doping rate exceeds 4%, carrier concentration and

mobility values decrease. When the tungsten doping rate is not added more than 4%, a positive change occurs in both electrical and optical properties [18].

2.5 Manufacturing Method

2.5.1 Hydrothermal Method

The hydrothermal method is frequently preferred due to the dilution capacity of water and aqueous solutions under normal conditions to dilute materials that cannot be dissolved at high temperatures and pressures. The parameters of both the production mechanism and the characteristics of the products obtained are pH, production time, production temperature and pressure. Autoclaves made of materials with high temperature and pressure resistance are used in the production with the hydrothermal method.

By using the hydrothermal production method, nanopowder materials can be produced in high temperature and pressure resistant autoclaves with hydrolysis reactions under normal conditions. Production with the hydrothermal method causes a significant increase in the rate of crystallization of the amorphous phase of materials. The solutions prepared for use in production with the hydrothermal method are in the form of suspension solution. Special equipment is not required to prevent temperature fluctuations in this method.

Hydrothermal method has some advantages over spin coating and spray sputtering methods. Uncontrolled crystallization can be formed at a degree close to the melting point of the material and high quality crystallization is achieved. The disadvantages of this method compared to other methods are that the equipment is expensive and the crystallization cannot be controlled during production. While it is necessary to pay attention in hydrothermal production, these values should be considered in order to eliminate the differences in liquid and gas form in the solution at the temperatures and pressures below the critical points. Salts used for production by hydrothermal method have higher solubility than oxides in solutions. These salts are called mineralizers.

In order to increase the efficiency of the production made by the hydrothermal method, the reaction environment should be well controlled and isolated from the external

factors. Recently, the hydrothermal method is frequently used in microwave, ultrasonic and electrochemical production methods.

CHAPTER 3

EXPERIMENTAL PROCEDURES

3.1 Sample Preparation

All chemicals used in the study were of analytical grade and were used as received without any further purification. The experimental procedure for the preparation of ZnO NSs was divided into two steps as shown in Fig.3.1.

Zinc acetate dihydrate (ZAD, ≥99.5%), monoethanolamine (MEA, ≥99.5%), hexamethylenetetramine (HEX, ≥99%), zinc nitrate hexahydrate (ZNH,98%), ethanol (EtOH, ≥99.9 %), dimethylformamide (DMF, 99.9%), and tungsten hexachloride (WCl_6, ≥99.9%), were obtained from Sigma-Aldrich and Merck. During all processes deionized water (DI) of resistivity with 18.2 mΩ cm^{-1} was used.

To remove the organic residue from the surface, the glass slides (25mm × 25 mm) were first washed in a detergent solution without cream, then sonicated for 5 min at EtOH and DI water, respectively. Lastly, glasses were treated by UV-ozone before and after the coating seed layer.

The seed solution was synthesized by dissolving ZAD in an EtOH solvent, and then an MEA stabilizer was added to the mixed solution. The concentration of ZAD in the ethanol solvent was 0.3 M, and the molar ratio of MEA to ZAD was maintained at 1:1 molar ratio. The final solution was stirred at 50 °C for 2 hours. Then the seed solution was deposited on glass substrates by spin coating technique (5000 rpm, 30 s). Cycles were applied to glass substrate five times, consisted of four components as spinning, drying, pre-heating, and cooling. Lastly, coated glasses were annealed at 500 °C for an hour.

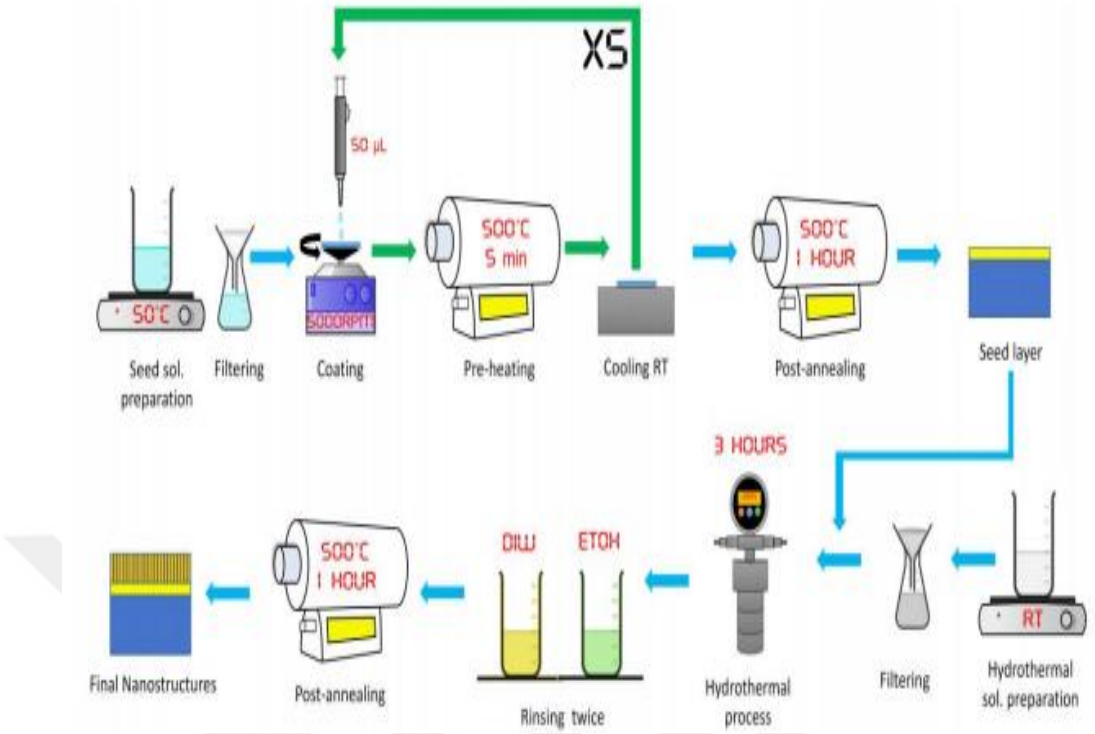


Figure 3.1 Schematic diagram of the experimental process

Briefly, a solution was prepared by dissolving a 0.02 M equimolar ratio of ZNH and HEX together in 200 ml DI water. WCl_6 was dissolved in DMF. Then, the solution was obtained to 40 mL of growth solution. The W dopant concentration ([molW]/[-molW+molZn]) was calculated to be at 1 %. The solution was magnetically stirred at 500 rpm for 1 hour at room temperature yielding a clear solution. The growth solution was transferred into a hydrothermal synthesis autoclave, which was then placed inside a pre-heated heating unit of maintained for 3 hours. Undoped ZnO NSs were grown at three different temperatures (75, 100, and 125^{o}C) and pressures (0.3, 0.5, 1 bar) while W-doped ZnO was synthesized at 100^{o}C and 1 bar. The thickness of the samples was estimated around 275 nm. The samples were labeled as ZO75, ZO100, ZO125, and WZO100, respectively. Then, samples were rinsed in DI water and EtOH twice, respectively. Finally, the samples were annealed at 500^{o}C for an hour.

The crystal structure of the films was investigated by the Rigaku Miniflex 600 Tabletop Powder X-ray diffractometer. The Raman spectra were collected using the Jasco NRS4500 in the range of 100 to 500 cm^{-1}. The optical transmittance and absorbance of the films were measured using a dual-beam UV–visible

spectrophotometer (SHIMADZU 1700) in the wavelength range of 300–1100 nm. Atomic force microscopy (AFM) was performed using a Quesant Q-Scope 250 microscope in noncontact mode and a 49 μm × 49 μm scanner. The electrical sheet resistance was measured at room temperature by the four-point probe method using Lucas Labs 302 and Keithley 2400 Sourcemeter. Grain size, shape, morphology, and structure of TFs were evaluated using scanning electron microscopy (Hitachi, high-vacuum FE-SEM SU5000). The specimens were coated with 4 nm of gold using a Leica EM ACE200 to observe microstructure at high magnification.

3.2 Characterizations

3.2.1 X-ray Diffraction (XRD)

XRD is a non-destructive technique used to determine the properties of the crystal structure of the material. X-rays come to the sample at an angle α. The primary beam is absorbed by the sample or transmitted through the sample; only the diffracted beam is recorded on the film (Figure 3.2). Diffracted beam occurs at twice the Bragg angle Θ_B.



Figure 3.2 Rigaku Miniflex 600 XRD measurement system

An example of XRD patterns measured for one of the deposited ZnO thin films is shown in the Figure 4. The detected diffraction peaks reveal the material has a crystal structure and its crystals are oriented in planes corresponding to the diffraction peaks. The peak of the highest density generally represents the preferred plane of crystal orientation. Each material has a standard XRD diffraction pattern (Joint Committee of Powder Diffraction Standards, JCPDS card), and the unknown material can be identified when the measured XRD pattern matches one of the JCPDS cards. For example, the measured XRD patterns of the deposited ZnO thin film match well with the JCPDS 00-036-1451 board, which belongs to the ZnO material of the hexagonal wurtzite structure. If the peak of diffraction is not detected, the material has an amorphous structure and cannot be identified using such measurements.

In addition to defining a material and its crystallinity, the following parameters can be estimated or defined from XRD data:

▪ The lattice constants a and c are estimated using formula [19]:

Equation 3.1: $$\frac{1}{d_{hkL}^2} = \frac{4}{3}\left(\frac{h^2+k^2+l^2}{a^2}\right) + \frac{l^2}{c^2}$$

▪ The crystal (grain) size, *D* is estimated using Scherer's formula [20]:

Equation 3.2: $$D = \frac{0.94\lambda}{\beta \cdot cos\,\Theta_B}$$

where **λ** is the wavelength of the XRD radiation source (= 1.541Å), β is the maximum half (FWHM) full width of the diffraction peak, and Θ_B is the Bragg angle.

▪ The crystal strain, ε is estimated using the formula [21]:

Equation 3.3: $$\varepsilon = \frac{c-c_0}{c_0}$$

where c and c_0 are the crystal constants of the deposited film and bulk material.

3.2.2 Scanning Electron Microscope (SEM)

SEM uses an electron beam (e-beam) to create a microscale magnified image of the sample.The image provides information about the scanning of the sample with a focused electron beam and the surface topography and the composition of the sample.

The most important advantage of using SEM over optical microscopes is that the sample can be examined in a larger surface area. The smaller electron wavelength compared to photons and the very high depth of field provide an advantage in scanning larger surfaces.

The microstructure surface topography of the stored films were examined using the HİTACHİ FE-SEM SU5000 brand SEM system (Figure 3.3). This device, which belongs to Yıldırım Beyazıt University Central Laboratory, can provide magnification from 40x to 250.000x. Throughout the generated images, the surface topography and particle size or shape (morphology) of a sample at nanometer resolution can be examined. Combined with EDX (Energy Dispersive X-moon Spectroscopy), it is possible to reveal the basic composition of any object studied and its distribution / mapping in the studied area. The EDX elemental composition can be expressed quantitatively as weight percent or atomic percent.



Figure 3.3 Hitachi, high-vacuum FE-SEM SU5000 brand SEM system

3.2.3 Atomic Force Microscope (AFM)

Atomic force microscope (AFM) is a characterization device that produces surface images according to the force differences on the surface, which has many modes, destructive and working in a destructive manner. AFM main components are probe and cantilever. The difference in force on the surface is detected by these two parts. AFM working principle, a laser beam is focused behind a console that has a tip interacting with a surface, and the beam is reflected in a four-quadrant photodetector. Normal forces between the tip and the surface deflect the console up or down. Lateral forces turn the console left and right. These deviations are measured by tracking the deflection of the reflected laser and used to create an image of the surface topography.

Q-Scope 250 brand AFM system (Figure 3.4) was used in this study to characterize the surface properties of zinc oxide transparent conductive oxide thin films. A non-contact scanning mode is used to create a 3-dimensional topological view of the sample surface. The XY sample stage of this system can accommodate a scan size of up to 50 µm x 50 µm. Also, the scanning resolution can be adjusted up to 800 dpi to reveal more surface detail. High image quality can provide information about many

parameters in image analysis, the most important of which are the root mean square (RMS) value of the surface roughness and the particle size and their histograms.

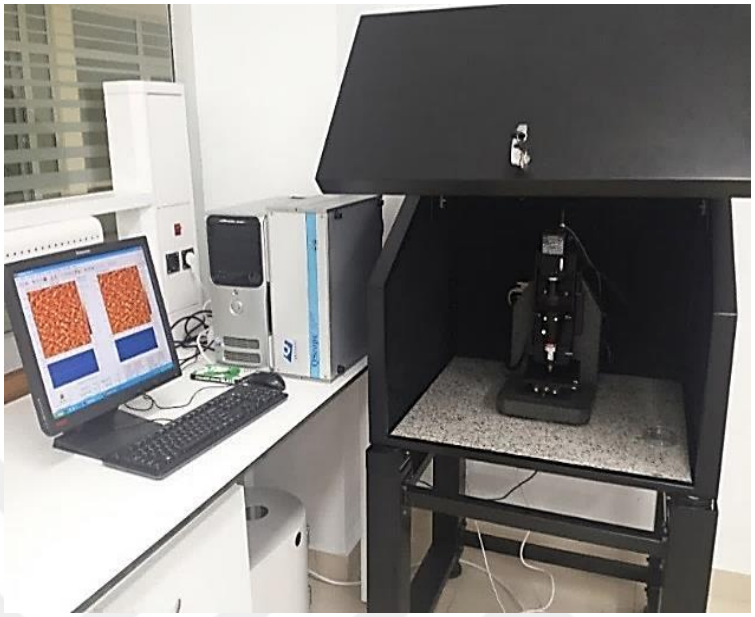


Figure 3.4 Q-Scope 250 brand AFM system

3.2.4 Raman Spectrometry

Raman Spectroscopy device is used in non-destructive characterization methods that provide information about the chemical structure, phase structure and morphological properties of materials. The working principle of the Raman Spectroscopy device is to analyze the light directed through the device by interacting with the atoms in the material.The wavelength of the scattered light is different from the laser sources generally used because it is critical to obtain information about the chemical structure of the material using different wavelengths.

Generally, Raman Spectroscopy devices provide in-depth information about the chemical structure of the material, just like fingerprint scanning, by analyzing the chemical structures of the materials in a fast and detailed manner. By making changes in the Raman spectrum of the Raman spectroscopy device, images can be taken in different combinations. In the images taken by changing the Raman spectrum, the morphology of the components and the changes in the phase distributions can be observed.

Raman Spectroscopy provides a very important distinction in terms of identifying a material and identifying it in others. Adjustments made in the Raman spectrum are one of the most important parameters in defining the properties of the material.

The density of the spectra is directly proportional to the concentration of the material. The most important parameters in the calibration of the device are to set the relationship between peak intensity and concentration well. After the calibration process is completed, routine and healthy measurements can be taken. The peak densities and absolute concentration values of the materials are critical in the measurements taken. In Figure 3.5 shows the Horiba brand Raman Spectrometer.

Spatial resolution and low micron values can be measured with the Raman Spectroscopy device. Raman Spectrometer analysis is useful for thechracterization of ZnO transparent and conductive oxide film.

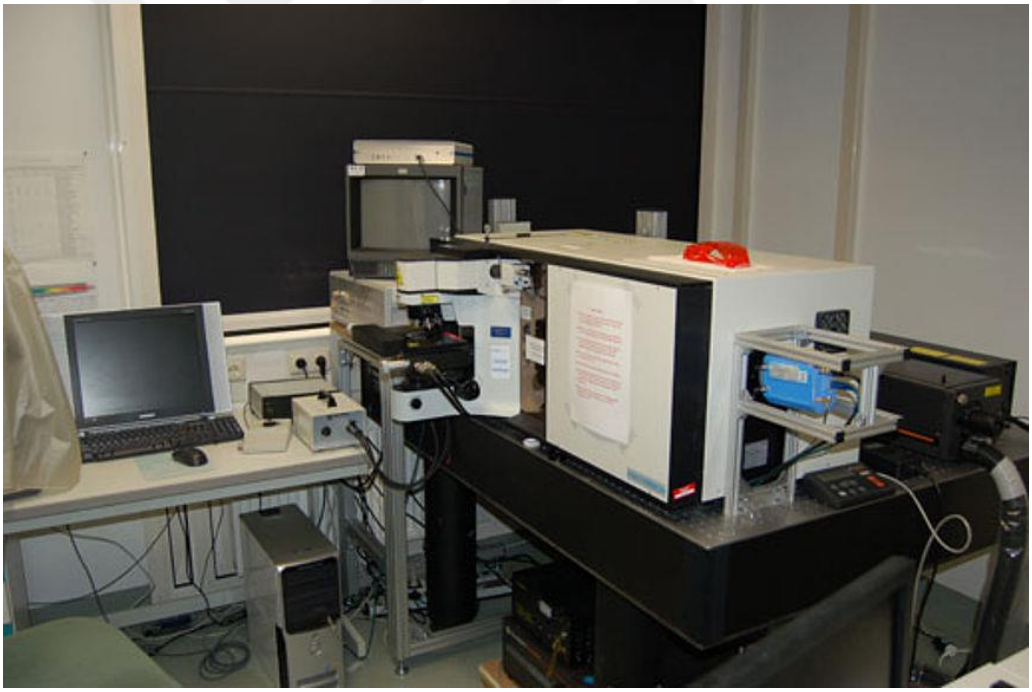


Figure 3.5 Horiba brand Raman Spectrometry [22]

CHAPTER 4

RESULTS AND DISCUSSION

4.1 Sample Preparation

In this study, first of all, the parameters were determined for the ZnO transparent and conductive oxide thin film that are planned to be produced. It was decided to determine the way to achieve optimum performance by examining parameters such as production method, temperature, doping and doping rate and pH.

First, seed layers were produced with the spin coating method. For seed layer production, The solution prepared for the seed layer was synthesized by dissolving ZAD with etOH and then the MEA stabilizer was added to the solution. The concentration of ZAD in the ethanol solvent was kept at 0.3 M and the molar ratio of MEA to ZAD at a 1: 1 molar ratio. The resulting solution was stirred at 50°C for 2 hours. Then, the seed solution was deposited on glass samples by spin coating technique (5000 rpm, 30 seconds). It consists of 4 parts as spinning, drying, preheating and cooling processes on glass samples. Finally, the coated glasses were annealed at 500°C for 1 hour.

Later, production was made with the hydrothermal method. In this production, aqueous growth solution was prepared by dissolving a mixture of 0.02M equimolar ratio ZNH and HEX in 200ml of DI water. 50 µL of NaOH was slowly dropped into the solution. The solution was magnetically stirred at 500 rpm for 1 hour at room temperature to obtain a clear solution. The growth solution was transferred to a hydrothermal synthesis autoclave, which was then placed in a preheated heating unit maintained for 3 hours. The samples were then rinsed twice with water and EtOH respectively. Finally, TFs were annealed at 500°C for 1 hour.

Finally, the characterization process was initiated in order to be able to choose between the samples produced. For characterization, examinations were performed on X-ray Diffraction (XRD), Atomic Force Microscope (AFM), Scanning Electron Microscope (SEM) and Raman Spectrocopy devices.

4.2 Characterization Results

4.2.1 X-ray Diffraction Results (XRD)

Figure 4.1 shows the XRD pattern of the NSs obtained in this study. The well-defined diffraction peaks are consistent with the growth of wurtzite structure of ZnO (JCPDS Data Card No: 036-1451). The high intensity of (002) reflection indicates that it is the preferred orientation of the crystallites for all the samples. The intensity of the peak gradually increases as the temperature of the hydrothermal process rises. The other peaks are owing to reflections from the (100) and (101) planes. These features suggest that the samples consist of polycrystalline nature.

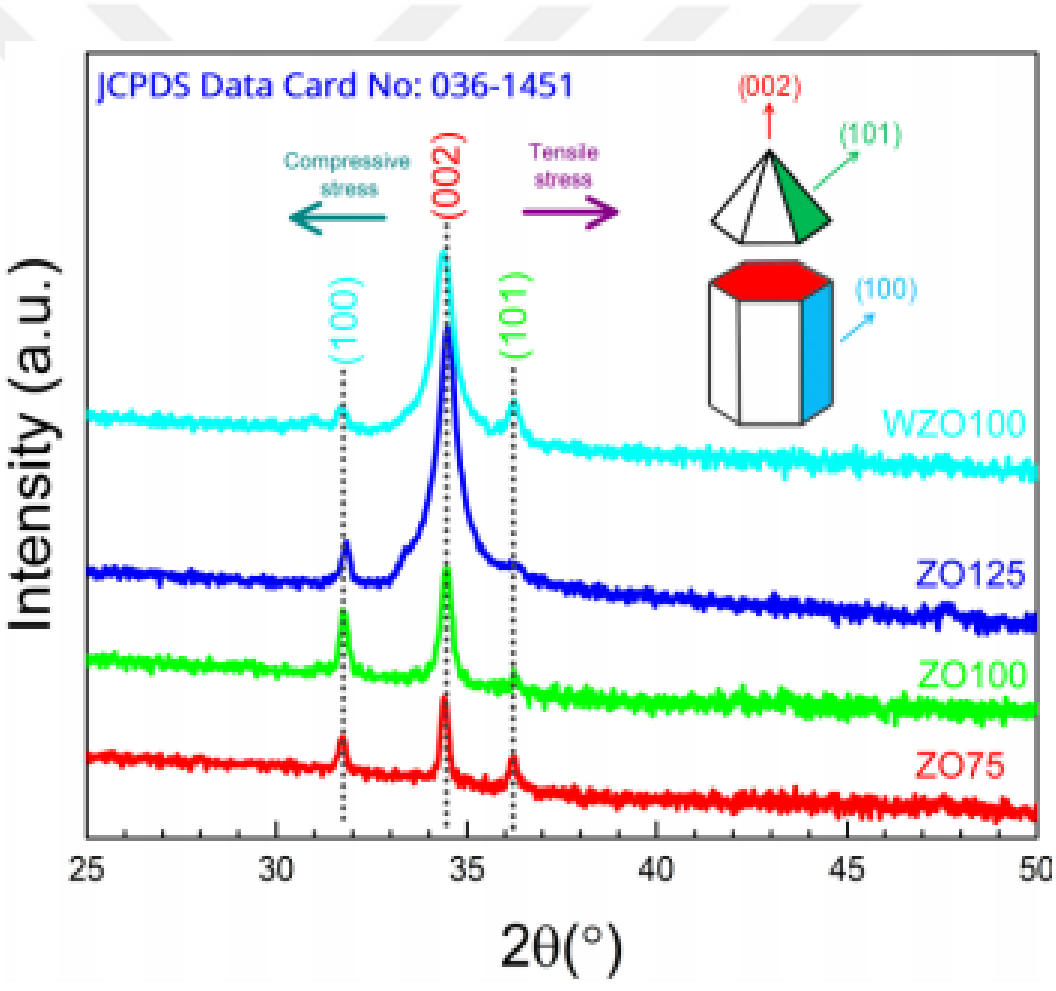


Figure 4.1 XRD pattern of ZnO NSs

Table 4.1 Parameters extracted from XRD and AFM measurements

SAMPLE	CRYSTALLITE SIZE (nm)	GRAIN SIZE (nm)	RMS (nm)
Z075	22.97	61.7	11.2
Z0100	29.88	64.4	2.3
Z0125	32.52	81.4	3.5
WZO100	40.93	159.5	47.6

4.2.2 Atomic Force Microscopy (AFM) Results

To shed some light on the importance of the deposition temperature affecting surface morphology of NSs, we carry out AFM measurements. Figure 4.2 depicts the 3D AFM topologies of the surfaces of NSs. The surface properties are specified with root mean square (RMS) roughness values that change with the temperature or dopant (Table 4.1). The value of RMS of the NSs is estimated to be as 11.16, 2.32, 3.54, and 47.61 nm for ZO75, ZO100 ZO125, and WZO100, respectively. With increasing temperature of hydrothermal process, the surface roughness firstly drops sharply and then slightly rises, however, the particle size shows a linear increasing trend with temperature. Larger particles are associated with higher surface roughness.

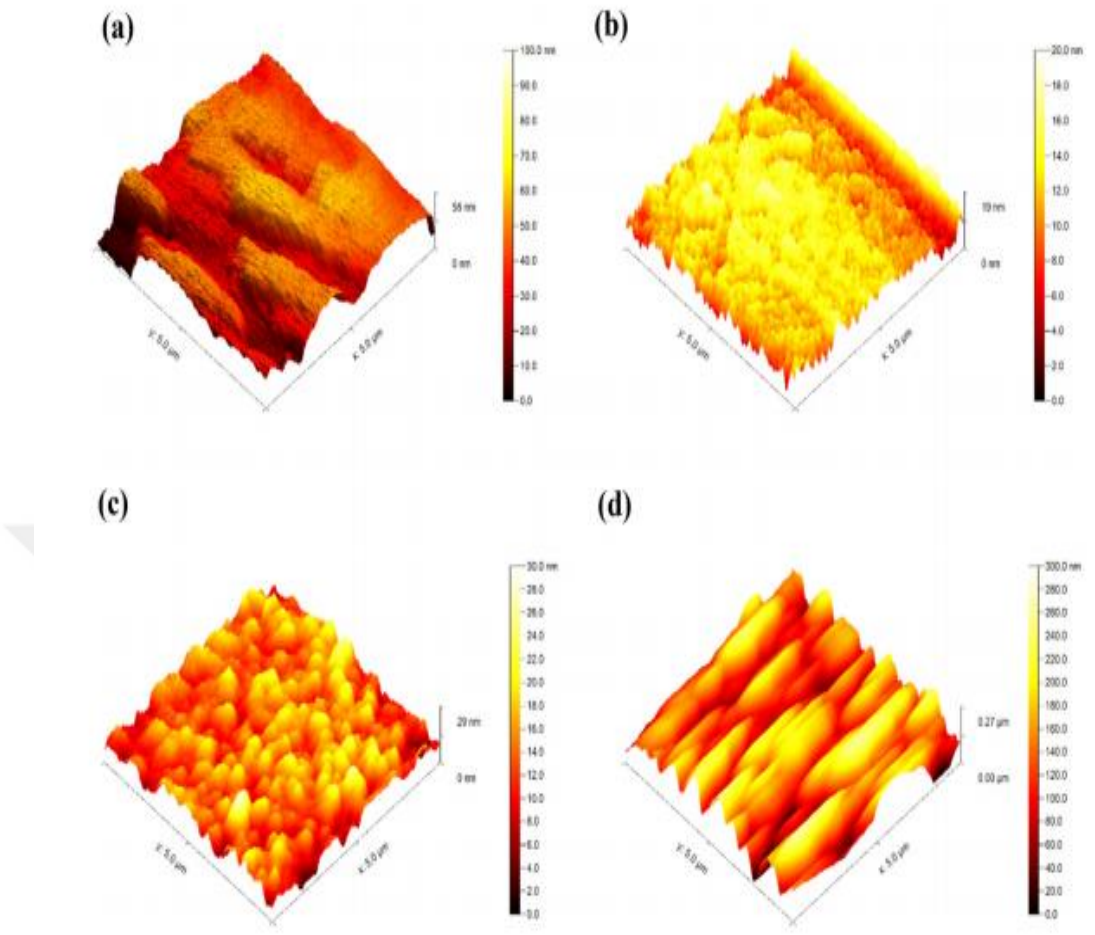


Figure 4.2 3D AFM topology of sample surfaces (a) ZO75, (b) ZO100, (c) ZO125, and (d) WZO100

It is possible to draw a clear conclusion regarding the growth temperature based on the above mentioned XRD and AFM data. The synthesis of the NSs at 100^{o}C which seems to be optimum among others is more appropriate, that is why ZnO is doped with W at this temperature. W-dopant directly changes the morphology of the NSs, RMS value dramatically increases. On the other hand, doping of W is more effective than increasing the temperature for having higher particle size.

4.2.3 Scanning Electron Microscopy (SEM) Results

The SEM images and the top diameter distributions are recorded to examine the morphology of the NSs, and the images acquired are presented in Figure 4.3. The EM Wizard software in the HİTACHİ FE-SEM SU5000 brand SEM system was used.More than 200 nanostructures were tested to determine the diameter distribution. The particle sizes were taken using ImageJ software. The quantitative analysis shows that the regions of top diameter distributions are enlarged, and the average top diameters increase with increasing growth temperature from 75 to 125^{o}C. When the growth temperature is 75^{o}C, obtained NSs have uniform diameters between 25–125 nm, and the average top diameter is 61.7 nm. The diameters of the NSs for a higher growth temperature (100^{o}C) are distributed in the range of 20–100 nm with the average top diameter of 64.4 nm. However, the region of distribution with the growth temperature of 125 ^{o}C ranges from 50 to 150 nm, and the average top diameter is 81.4 nm. As shown in Figure 10d and h, nanostructures transformed from rod to plate and growth plates intertwined with each other. Among all the samples, the most regular hexagonal structure was observed for WZ100. The distribution for WZ100 is between 50 and 400nm, and the average top diameter is 159.5 nm. The crystalline and particle sizes of films obtained from XRD, AFM, and SEM analyses are in great agreement with each other, respectively. Their values based on these measurements vary in the same fashion.

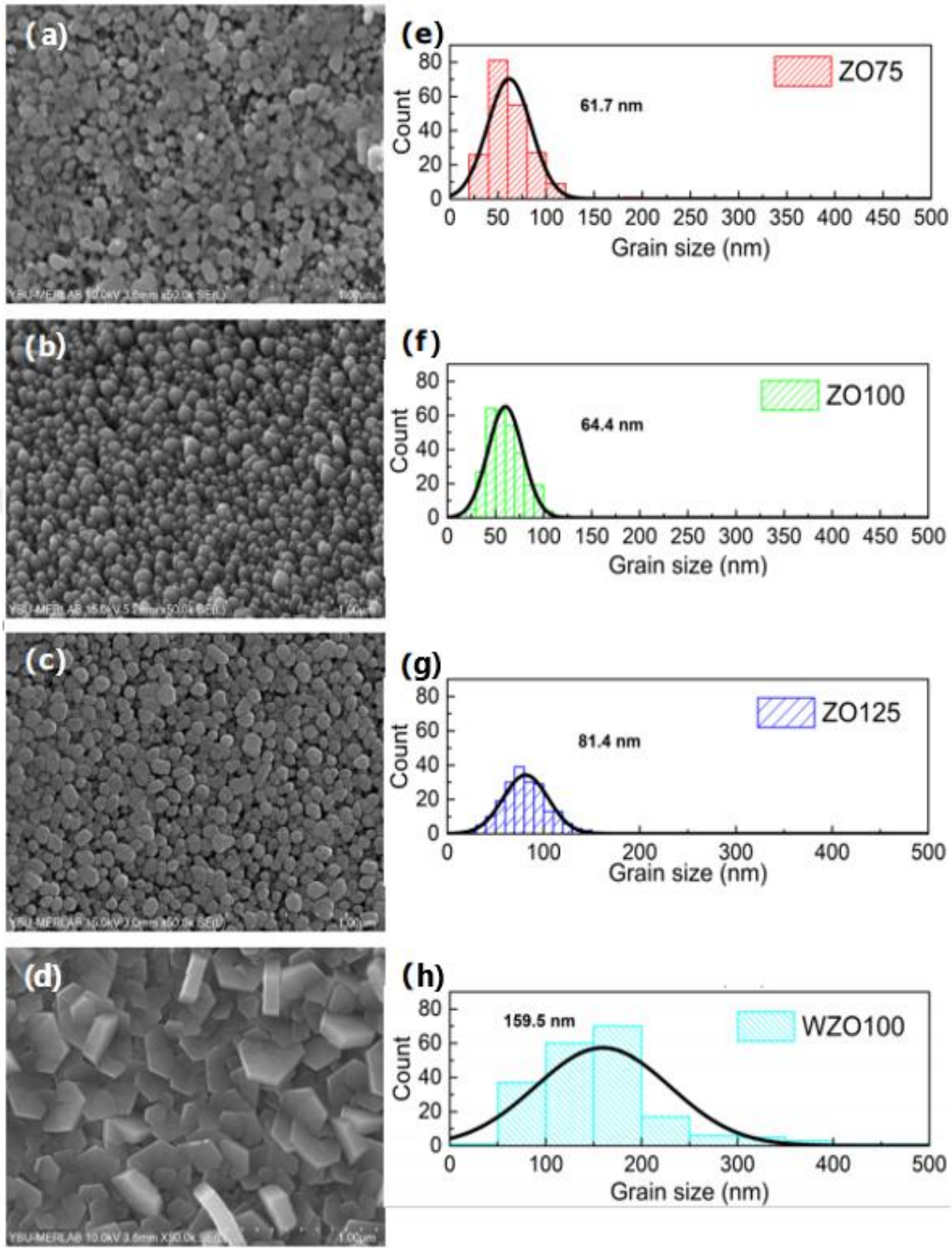


Figure 4.3 SEM image of the NSs (a) ZO75, (b) ZO100, (c) ZO125, and (d) WZO100. The size distribution histograms obtained from the SEM images for samples: (e) ZO75, (f) ZO100, (g) ZO125, and (h) WZO100.

4.2.4 Raman Spectroscopy Results

The Raman spectra and a Lorentzian function to fit the Raman band having a peak around 435 cm-^{1} for the NSs are shown in Fig 4.4a and Fig 4.4b, respectively. Wurtzite structured ZnO, one of the simplest uniaxial crystals, belongs to the C^{6}_{4v} space group. For the perfect ZnO crystal, only the optical phonons at Γ point of the Brillouin zone are involved in first-order Raman scattering. Group theory predicts the existence of the following optic modes: $\Gamma=A_1+2B_1+ E_1+E_2$ where, both A_1 and E_1 modes are polar and split into transverse optical (A_1^{TO} and E_1^{TO}) and longitudinal optical (A_1^{LO} and E_1^{LO}) components. E_2 mode consists of two modes of low and high-frequency phonons (E_2^{low} and E_2^{high}), which are associated with the vibration of the heavy Zn sublattice and oxygen atoms, respectively. B_1 modes are silent, i.e. both IR and Raman are inactive. All the modes mentioned above are first-order Raman-active modes according to the Raman selection rule [23].

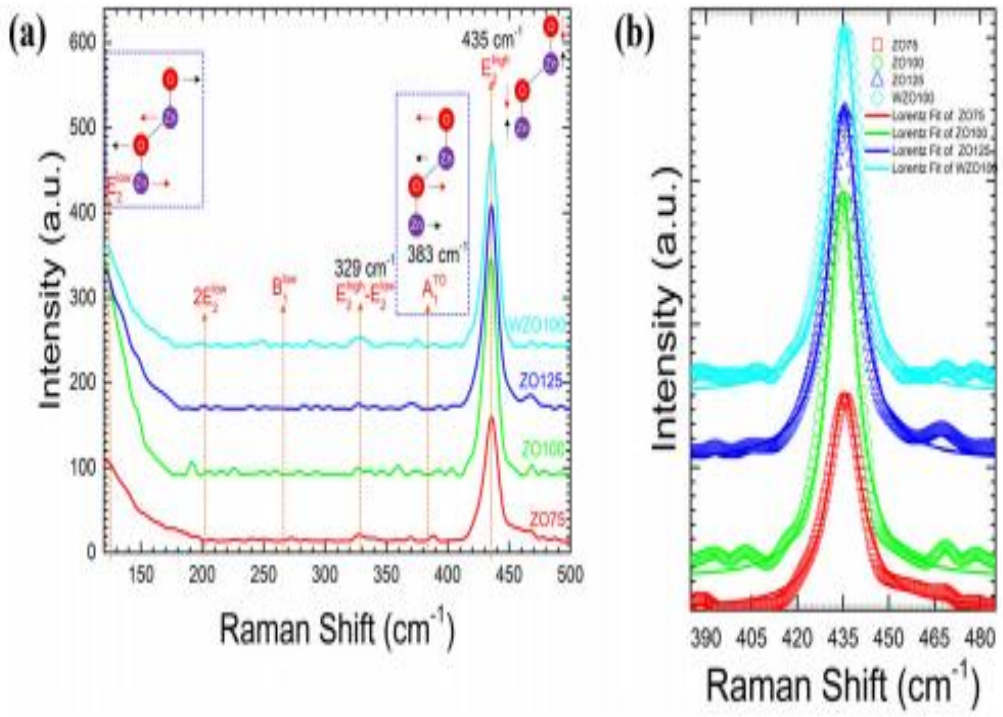


Figure 4.4 4 a) Raman spectra of samples, b)Lorentzian fitted peaks of 435 cm^{-1}

In the present study, three clear phonon modes are observed for the NSs at ~100, 330, and 435 cm^{-1}. As shown in Figure 4.4, Raman spectra of the NSs consists of high intensity non-polar E_2 optical mode at ~100 (E_2^{low}) and 435 (E_2^{high})cm^{-1} and peak due to the multi-phonon process (E_2^{high}- E_2^{low}) at 327 cm^{-1}. Low-intensity peaks at around 378 cm^{-1} and 407 cm^{-1} are commonly assigned to A_1^{TO} and E_1^{TO} modes of ZnO. As listed in Table 3, the frequencies (~435 cm^{-1}) and the Γ (~11cm^{-1}) of the E_2^{high} mode for the NSs exhibit a little deviation. Shifts of peak position refer to strain, stress, and deformations [23].

Table 4.2 Peak parameters are estimated from the fitting Lorentzian function of E_2^{high} mode.

SAMPLES	ω_0 (cm^{-1})	Γ (cm^{-1})	I_{max} (a.u.)	Γ_a/Γ_b
Z075	435.13	11.90	126.60	1.07
ZO100	434.43	11.89	241.34	1.17
Z0125	434.95	11.47	214.99	1.16
WZ100	434.99	12.13	231.83	1.08

ω_0: peak position, Γ: FWHM, I_{max}: peak intensity, Γa/Γb: asymmetry ratio

The Raman band shifts to either lower or higher wavenumber side depending on whether the strain is tensile or compressive, respectively. The highest tensile stress is shown at the sample of ZO100. FWHM value is helping to understand the doping effect and crystalline quality, for higher values of FWHM, the impurities increase while crystalline quality reduces. It is a measure of the crystal perfection of ZnO. WZ100 has the highest value of FWHM.

4.2.5 Ultraviolet-Visible Spectroscopy

4.2.5.1 Optical Characterization Results

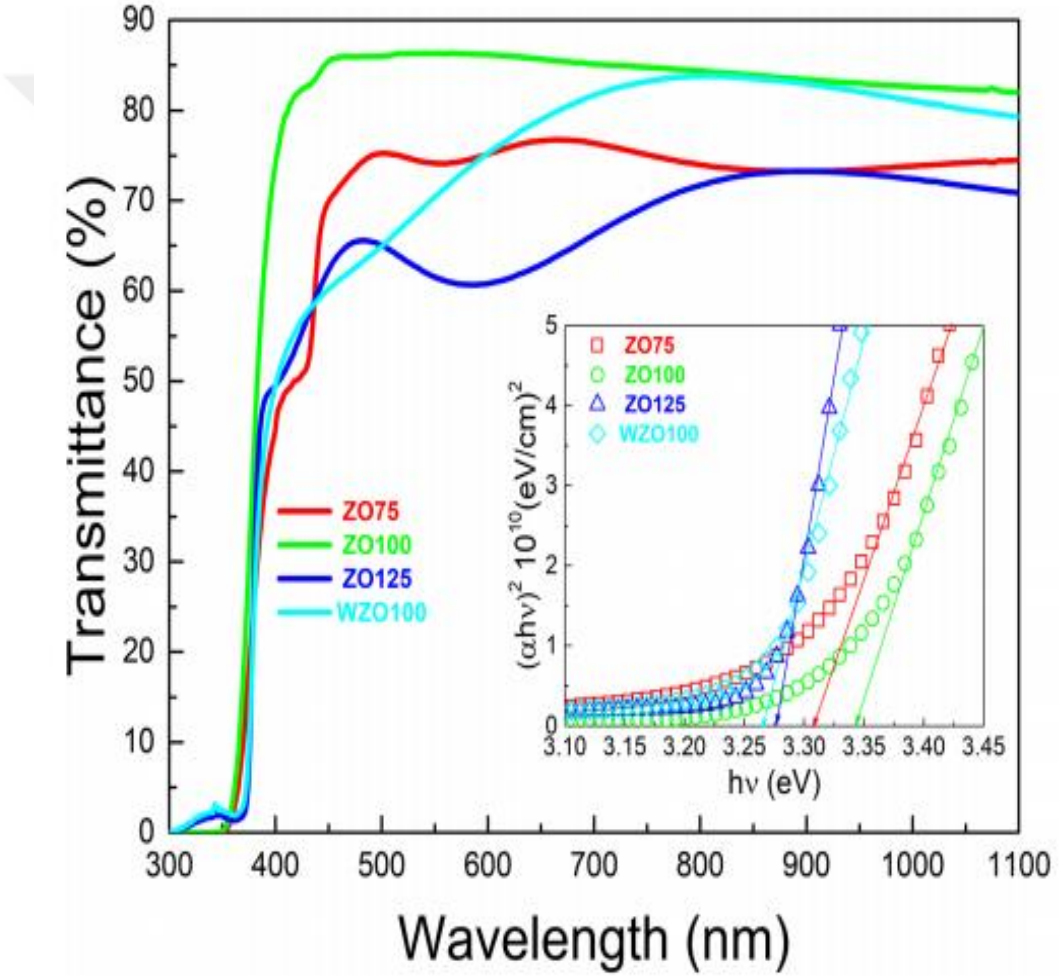


Figure 4.5 Optical transmittance of the NSs as a function of wavelength. The inset shows a Tauc plot of the optical transmittance spectra of the NSs.

Optical transmittance (T) measurements were performed to examine the band gap of NSs. The permeabilities of ZO75, ZO100, Z0125 and WZO100 samples produced by the hydrothermal method were found to be 75.26%, 85.73, 61.77 and 69.48%, respectively. As seen in Figure 4.5, it is seen that the average transmittance is between 400 nm and 700 nm. When the results are examined, it is observed that the permeability rate in the undoped samples increases with the temperature increase, and then decreases after it. The unadulterated samples are reference samples. W-doping was done by choosing the optimum value among these samples. ZO100 sample has the most optimum value with 85.73% permeability. It is seen that the permeability rate decreased to 69.48% after doping.

4.2.5.2 Electrical Characterization Results

The inset of Fig. 4.5 depicts $(ahv)^2$ versus (hv) plot of the NSs for the determination of bandgap (E_g) value. The value of E_g is estimated as 3.31, 3.34, 3.27 and 3.26 eV for ZO75, ZO100, ZO125, and WZO100, respectively. This finding is opposed to those given by Mohd Fudzi [20] et al. who found that band gap is relatively lower at 100^{o}C, which disrupts the trend of the narrowing band gap with increasing temperature.After W-doping at 100^{o}C, band gap further reduces which might be due to many body effects (band gap shrinkage) as we reported before [24].At higher doping concentrations, electron–electron interactions particularly become important, leading to band gap shrinkage [24].

Further analysis reveals that the deposition temperature and W-dopant can significantly influence the electrical properties. To analyze the electrical properties of the NSs, the sheet resistance (Rsh) is calculated using the equation of $R_{sh} = \left({}^{\pi}/_{ln\,2}\right)^{{}^{\Delta V}/_{I}}$, where $({}^{\pi}/_{ln\,2})$= 4.532 is the correction factor, I and ΔV are the measured current and potential differencebetween the voltage probes, respectively. The observed values of sheet resistance vary between 12.38 and 156.80 mΩ/sq for undoped NSs.R_{sh} considerably decreases with the deposition temperature since the crystal quality and surface flatness are improved. Moreover, it is noteworthy that Rsh dramatically reduces to 0.22 from 102.2 mΩ/sq after W-dopant at 100^{o}C. This is presumably due to freeelectron contribution of W-doping after occupying W^{+6} to locations of Zn^{+2} in ZnO lattice.

Finally, the figure of merit value (FOM), which is generally realized as a performance parameter for transparent conductive oxides, of the NSs was calculated. To evaluate FOM, we consider the equation $FOM = [-\frac{1}{R_{sh}\, ln(T)}]$ proposed by Gordon [25].

Note that our growth temperature values fall into the common temperature range employed to grow ZnO nanostructures during the hydrothermal process [26]. Furthermore, we noticed that the best growth temperature region for our solution under the experimental conditions take place between 75 and 125^{o}C after examining different growth temperatures. By adjusting growth temperature, we achieved to get uniform structures via hydrothermal route. A significant change was observed in all properties of the films as the growth temperature is tailored. In our case, we reached favorable conditions for better figure of merit associated with a high transmittance and low resistance of the films at 100^{o}C. Therefore, we also grown W-doped ZnO at 100^{o}C, yielding an impressive figure of merit by accomplishing appreciably low sheet resistance value. It is found to be as 0.0224, 0.0636, 0.168, and 12.48 $\mu\Omega^{-1}$ for ZO75, ZO100, ZO125, and WZO100, respectively. The value first increased gradually with the deposition temperature changing from 75 to 100^{o}C and then jumps appreciably at 125^{o}C. When adding W-dopant, it further increases. Even though there is a wide range of the value FOM in the literature to interpret the data, our values are mostly comparable with those given in the literature [27,28]. However, their values are respectively lower. The underlying reason is that the present NSs exhibit relatively higher sheet resistance despite their satisfactory optical properties. One possible solution to this issue is to tailor amount of W-doping, which can provide an improvement in mobile carrier concentration within the ZnO lattice and therefore rise the FOM.

CHAPTER 5

CONCLUSION AND RECOMMENDATIONS

Finally, comparatively undoped and W-doped samples were produced to obtain NS structures from ZnO. Hydrothermal method is preferred in the production of transparent and conductive oxide thin films and it is aimed to diversify the studies in the literature with the production method. The produced transparent and conductive ZnO thin films were compared in many parameters. It is aimed to reach optimum values by examining temperature, doping, doping rate and pH parameters. When the properties of the optimum sample obtained were examined, NSs were characterized to control their structural, morphological, optical and electrical properties. XRD, AFM, SEM, Raman Spectroscopy and UV-Spectroscopy instruments were used for characterization. When the samples were examined, it was seen that the change in the precipitation temperature directly affected all the monitored parameters. In the XRD analysis, it was observed that the peak intensity value increased as the temperature increased in the undoped ZO75, ZO100, Z0125 samples. It has been determined that the RMS value, which is one of the most important parameters in AFM analysis, is the optimum value among the reference samples in the undoped ZO100 sample. In the SEM and Raman spectrometer results, it was determined that the most optimum values were the pure ZO100 sample. In the UV-Visible analysis, it was determined that the ZO100 sample was the most optimum value in its optical and electrical properties. It has been determined that the ZO100 sample has a permeability rate of 85.73% and a band gap value of 3.34 eV. The FOM values of the produced samples increased from 0.0224 $\mu\Omega^{-1}$ to 12.48 $\mu\Omega^{-1}$ after W doping. In the light of the results obtained, it has been observed that the production of W-doped ZnO by hydrothermal method can be a serious alternative in the search for alternatives for transparent and conductive oxide thin films. Its easy production, good performance and low production cost will create numerous opportunities for the manufacture of various optoelectronic devices.

REFERENCES

[1] M. Hiramatsu, K. Imaeda, N. Horio, and M.Nawata, J. Vac. Sci. Technol., A 16 p. 669 (1998).

[2] C.G. Van de Walle, Phys. Rev. Lett., **85,** 1012 (2000).

[3] Global Transparent Conductive Films Market: Industry Analysis and Forecast (2019-2027) by Application, Material, and Region.Retrieved July 13,2021 from https://www.maximizemarketresearch.com/marketreport/globaltransparentconductive-films-market/30899/#toc

[4] Transparent Conductive Films Market by Technology (ITO on PET, ITO on Glass, Non ITO oxides, Silver Nanowires, Graphene, Carbon Nanotube, Metal Mesh, Micro fine Wire, PEDOT) and Application (Smart Phones, Tablets and tablet PCs, Notebooks, All-in-one PCs, TV Displays, OLED lighting, OPV and DSSCs) - Global Opportunity Analysis and Industry Forecast, 2013 – 2020. Retrieved July 13,2021 from https://www.alliedmarketresearch.com/transparent-conductive-filmsmarket

[5] A.C.Scheinost, Swiss Federal Institute of Technology (ETH), Zurich, Switzerland, Metal Oxides

[6] Izyumskaya, N., Avrutin, V., Özgür, Ü., Alivov, Y. I., & Morkoç, H. (2007). Preparation and properties of ZnO and devices. Physica Status Solidi (b), 244(5), 1439-1450.

[7] Ohtomo, A., Kawasaki, M., Koida, T., Masubuchi, K., Koinuma, H., Sakurai, Y., ... & Segawa, Y. (1998). MgxZn1− xO as a II–VI widegap semiconductor alloy. Applied Physics Letters, 72(19), 2466-2468.

[8] Jin, Y., Zhang, B., Yang, S., Wang, Y., Chen, J., Zhang, H., ... & Chang, R. P. (2001). Room temperature UV emission of MgxZn1−xO films. Solid State Communications, 119(6), 409-413.

[9] Stavola, M., Weber, E. R., & Willardson, R. K. (1998). Identification of defects in semiconductors. Elsevier Science.

[10] Hu, J., & Gordon, R. G. (1992). Textured aluminum-doped zinc oxide thin films from atmospheric pressure chemical-vapor deposition. Journal of Applied Physics, 71(2), 880-890.

[11] Hu, J., & Gordon, R. G. (1992). Atmospheric pressure chemical vapor deposition of gallium doped zinc oxide thin films from diethyl zinc, water, and triethyl gallium. Journal of Applied Physics, 72(11), 5381-5392.

[12] Mohamed Nouri Sbeta. Integration of sol-gel derived doped zinc oxide films and solution-processed metal nanoparticles for thin film photodiode and solar cell applications. (2019)

[13] Mechanical Properties and Microstructure of Zinc Oxide Varistor Ceramics. Retrieved July 13,2021 from https://www.ipen.br/biblioteca/cd/ptech/2005/PDF/15-08.pdf

[14] Jagadish, C., & Pearton, S. J. (Eds.). (2011). Zinc oxide bulk, thin films and nanostructures: processing, properties, and applications. Elsevier.

[15] Cerrato, E.; Gionco, C.; Berruti, I.; Sordello, F.; Calza, P.; Paganini, M.C. Rare earth ions doped ZnO: Synthesis, characterization and preliminary photoactivity assessment. J. Solid State Chem. 2018, 264, 42–47.

[16] Faisal, M.; Ismail, A.A.; Ibrahim, A.A.; Bouzid, H.; Al-Sayari, S.A. Highly efficient photocatalyst based on Ce doped ZnO nanorods: Controllable synthesis and enhanced photocatalytic activity. Chem. Eng. J. 2013, 229, 225–233.

[17] Pan Jiaojiao, Wang Wenwen, Wu Dongqi, Fu Qiang, Ma Ding (2016) Tungsten Doped Indium Oxide Thin Films Deposited at Room Temperature by Radio Frequency Magnetron Sputtering

[18] Pan, F.; Luo, J.; Yang, Y.; Wang, X.; Zeng, F. Giant piezoresponse and promising application of environmental friendly small-ion-doped ZnO. Sci. China Technol. Sci. 2012, 55, 421–436.

[19] Yildiz, A., Cansizoglu, H., Turkoz, M., Abdulrahman, R., Al-Hilo, A., Cansizoglu, M. F., ... & Karabacak, T. (2015). Glancing angle deposited Al-doped ZnO nanostructures with different structural and optical properties. Thin solid films, 589, 764-769.

[20] Tsay, C. Y., Fan, K. S., & Lei, C. M. (2012). Synthesis and characterization of sol–gel derived gallium-doped zinc oxide thin films. Journal of alloys and compounds, 512(1), 216-222.

[21] Y. Huang, M. Liu, Z. Li, Y. Zeng, S. Liu, Raman spectroscopy study of ZnO-based ceramic films fabricated by novel sol–gel process, Materials Science and engineering: B 97(2) (2003) 111-116.

[22] GFZ German Research Centre For Geoscıences from https://www.gfz-potsdam.de/en/section/chemistry-and-physics-of-earthmaterials/infrastructure/raman-spectroscopy-laboratory

[23] Z.Zhaochun, H. Baibiao, Y. Yongqin, C. Deliang, Electrical properties and Raman spectra of undoped and Al-doped ZnO thin films by metalorganic vapor phase epitaxy, Materials Science and Engineering: B 86(2) (2001) 109-112.

[24] L. Mohd Fudzi, Z. Zainal, H.N. Lim, S.-K. Chang, A.M. Holi, Effect of temperature and growth time on vertically aligned ZnO nanorods by simplified hydrothermal technique for photoelectrochemical cells, Materials 11(5) (2018) 704.

[25] A. Yildiz, E. Ozturk, A. Atilgan, M. Sbeta, A. Atli, T. Serin, An understanding of the band gap shrinkage in Sn-doped ZnO for dye-sensitized solar cells, J Electron Mater 46(12) (2017) 6739-6744.

[26] R.G. Gordon, Criteria for choosing transparent conductors, MRS bullet in 25(8) (2000) 52-57.

[27] S. Baruah, J. Dutta, Hydrothermal growth of ZnO nanostructures. Sci. Technol. Adv. Mater. 10(1), 013001 (2009)

[28] W. Battal, M. Rouchdi, H. Shaili, M. Ouafi, R. Essajai, A.Belafhaili, N. Hassanain, A. Mzerd, Strontium doping effect on characteristics of ultrasonically sprayed zinc oxide thin films. Appl. Phys. A 126(7), 1–10 (2020)